Chapter III
Fundamentals

AOD refining is based upon:

- o CO Dilution
- o Mixing
- o Degassing

Each of these AOD phenomena and a reaction mechanism are discussed herein.

A. CO Dilution

During historical stainless steel decarburization by conventional oxygen blowing, the atmosphere in equilibrium with the melt is essentially pure CO at one atmosphere pressure. Under these conditions, the amount of chromium existing in the melt is limited by equilibrium with a given carbon content at a given temperature. The curves shown in Figure 2 illustrate these equilibrium effects. Any excess of chromium is rapidly oxidized. As the carbon content of the melt decreases, the amount of chromium also decreases. Raising the melt temperature raises the equilibrium chromium concentration, but temperatures are soon reached which are uneconomically high in terms of refractory life.

These relations which establish the extent to which the melt can be decarburized without oxidizing chromium have been reported by several investigators[21,22,23,27,28]. The thermodynamic relationships are discussed in those references and are reviewed in detail in other texts. The oxygen level of the bath is controlled by the most stable oxide of chromium (after the more stable oxides such as silicon and aluminum have been removed). Equation [1] shows the chemical equation for carbon removal together with its equilibrium constant assuming that Cr_3O_4 is the most stable oxide.

$$1/4\ Cr_3O_4\ (s) + \underline{C} = 3/4\ \underline{Cr} + CO\ (g) \qquad [1]$$

$$K = \frac{(a_{Cr})^{.75}\ (P_{CO})}{(a_{Cr_3O_4})^{.25}\ (a_C)}$$

(There are some reservations concerning whether Cr_3O_4 is the most stable oxide at steelmaking temperatures; those considerations are beyond the scope of this text.)

In similar studies for high-chromium ferroalloys, Krivsky (1) used argon-oxygen mixtures to study decarburization. He found that, if argon was injected along with the oxygen, the argon diluted the CO evolved and thereby decreased its partial pressure. This favors the carbon-oxygen reaction and increases greatly the amount

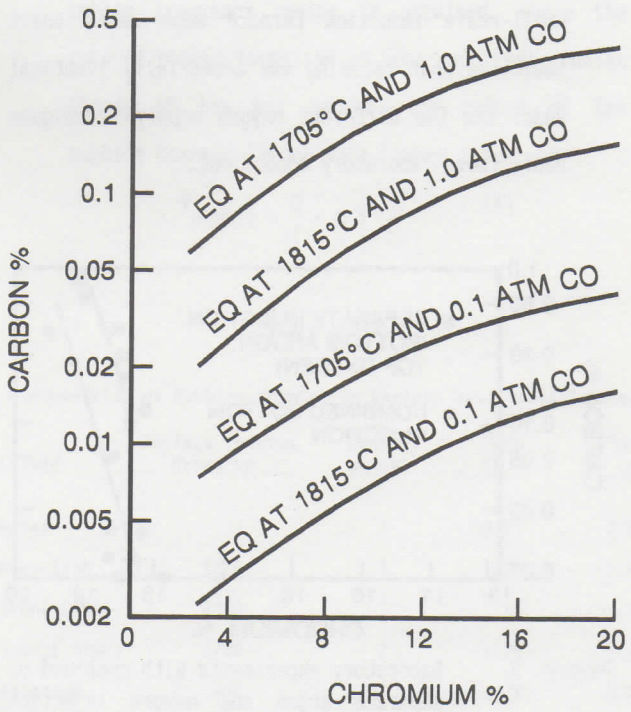

Figure 2. Carbon - chromium equilibrium curves.

of chromium which can be retained in the melt at practical temperatures.

Although equilibrium relationships provide an adequate picture of the direction in which a process will move, they do not indicate the actual path or rate of the reactions. Remember that gaseous diatomic oxygen first dissolves as monatomic oxygen in the molten metal. Equations [2] and [3] break down equation [1] into the two reactions believed to be controlling the over-all equilibrium.

$$1/4\ Cr_3O_4\ (s) = 3/4\ \underline{Cr} + \underline{O} \qquad [2]$$

$$\underline{C} + \underline{O} = CO\ (g) \qquad [3]$$

$$1/4\ Cr_3O_4\ (s) + \underline{C} = 3/4\ \underline{Cr} + CO\ (g) \qquad [1]$$

As written, they show that oxygen is absorbed by the melt before it reacts with carbon and subsequently leaves the system as CO. Top blown oxygen-bottom blown argon tests have shown that this reaction sequence does, in fact, occur (see the appended reference by Choulet, Death and Dokken). Figure 3 shows a comparison of separate injection with combined bottom injection in small-scale induction furnace experiments which indicates that refining was essentially identical under the two different oxygen supply techniques under those laboratory conditions.

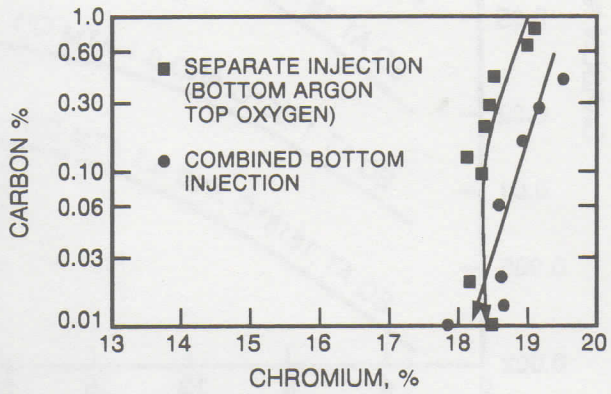

Figure 3. Laboratory experiments with combined or separate argon and oxygen injection. (Choulet, Death and Dokken (26))

Figure 4 shows the results of laboratory induction furnace tests using several dilution ratios. For a given dilution ratio, it was found that there were distinct break points in the decarburization reaction where the oxygen efficiency for carbon removal dropped rapidly and more chromium and other metallic oxidation occurred. These break points were related to equilibrium carbon monoxide pressures at the test composition and temperature, and it was found that this calculated pressure could not be predicted by assuming 100 per cent conversion of the input oxygen to carbon. With a mixture of oxygen and argon in the proportions of 1:2, for example, the break point did not occur at a calculated pressure of 0.50 atmosphere. However, it was found that for any given gas mixture the carbon level at which this decrease in decarburization rate occurred was reproducible and predictable[2].

Consideration of these results led to the development of the programmed blow. This involves increasing the oxygen dilution during decarburization so that continually lower carbon levels can be obtained without excessive chromium

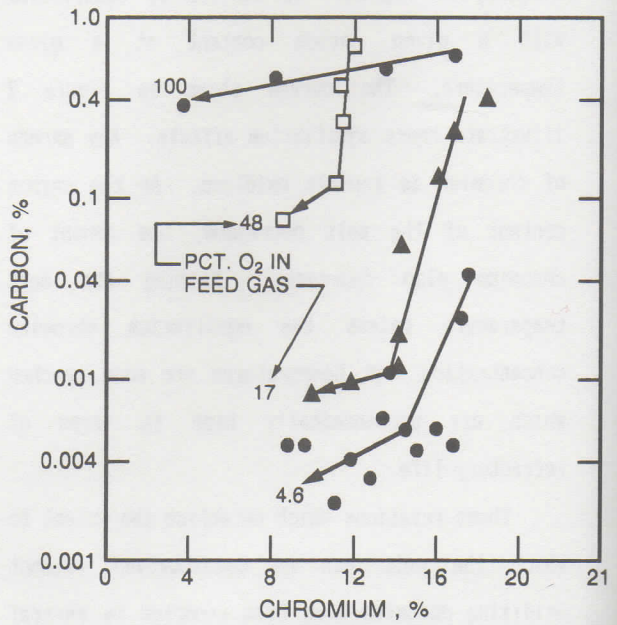

Figure 4. Effect of dilution ratio on carbon content. (Choulet, Death and Dokken (26))

oxidation. The consequences of this improvement were that the optimum proportion of argon can be determined and used for the instantaneous carbon and chromium content. This would require continually changing oxygen/argon proportions for minimum argon usage. It was found that this could be approximated by two or more stepwise changes in gas ratios.

In summary, decarburization of stainless melts containing specification levels of chromium can be accomplished. Through variation of the diluent gas volume, excessive oxidation of chromium and attendant bath temperature increase can be controlled. The need for low-carbon ferrochromium in stainless steel production is thereby eliminated. A review of AOD fundamentals is included in the appended reference by Choulet, Death and Dokken[26].

B. Mixing

The submerged injection of gases into molten metals is an intrinsic aspect of most metal refining operations. With the increase in the number of ladle steelmaking operations, the theoretical and industrial aspects of submerged gas injection have been considered at some length at a number of recent symposia, especially the Scaninject conference[29,30]. Gases are injected into the AOD vessels through tuyeres located in the lower side wall. A thorough review of tuyere design, especially as it relates to other processes, can be found in volume I of this series. There have been many studies on the hydrodynamic phenomena associated with submerged gas jets in liquid metals; generally these studies have used aqueous systems as a means of predicting jet and bubble behavior in molten metals.

Investigations have shown that there is a large difference in the physical behavior of bubbles and jets between gases in water and liquid metals[31,32,33,34,35]. The bubbles that form on the tip of the tuyere in liquid metal systems are larger than those formed in aqueous systems. This is primarily due to the non-wettability of the tuyeres in liquid metal systems. Jet penetration in liquid metals is much less than the jet penetration of gases in water. For a very complete description of jet penetration in liquid metal please refer to Brimacombe and co-workers[31,35].

Gases injected into molten metals are believed to form very large spherical-capped bubbles due to the high surface tension of liquid metals. Sahai and Guthrie[35] have calculated the minimum theoretical volume of a bubble forming on a 3 mm orifice in water, iron, steel, aluminum, and copper. These calculated bubble volumes are shown in Table I. It is clearly evident that the minimum bubble size forming at an orifice is much larger in molten metal systems than aqueous systems.

At low flows, the sum of bubble volumes remains constant. At sufficiently higher flows, surface tension is less important and a constant bubble frequency regime is attained, where the rate of bubble formation in iron and steel remains steady at ten per second. The volume of the bubbles becomes larger with higher flows per:

$$V_{bubble} = \frac{Q}{f} \tilde{=} 0.1\ Q \qquad [4]$$

TABLE I[36]

Minimum size of Bubbles forming in Various Gas/Liquid Systems

Liquid	Surface Tension dynes/cm	Density gm/cm^3	d_{min} cm	V_{min} cm^3
Water	73	1	0.51	0.07
Pure Iron	1788	7	1.77	2.89
Iron(.05%S)	1350	7	1.54	1.90
Steel(.01%C)	1760	7	1.75	2.82
Aluminum	900	2.37	2.16	5.24
Copper	1280	8.24	1.38	1.37

The size of bubbles in molten iron, water, and mercury was estimated by Sano and Mori[37,38] to be,

$$d = .091 \left(\frac{J}{P_1}\right)^{.50} \times V_s^{.44} \quad [5]$$

where d is the diameter; J, surface tension of the liquid; P_1, density of the liquid; and V_s, bubble rise velocity. Using equation [5], the average bubble diameter for a typical AOD operation is 10 cm.

By equating the energy supplied to the bath by rising bubbles to turbulent energy losses in the bath, Sahai and Guthrie[39] predicted the following relationship for plume velocity, U_p,

$$U_P \propto \frac{Q^{.33} L^{.25}}{R^{.33}} \quad [6]$$

where Q is the gas flowrate at the mean height and temperature of the bath; L, the bath depth; and R, the vessel radius. The plume velocity is the velocity of the gas-liquid region (bubble plume) as it rises up through the liquid. They also equated the bubble rise velocity to the plume velocity, and determined the following relationship for the average recirculation speed in the vessel, u,

$$u \propto \frac{U_P}{R^{.33}} \quad [7]$$

The mixing time in a vessel should be inversely proportional to the recirculation speed;

$$t \propto \frac{1}{u} \quad [8]$$

From equations [6] and [7], it follows then that the mixing time should be inversely proportional to $Q^{1/3}$.

$$t \propto Q^{-.33} \quad [9]$$

Equation [9] should be kept in mind when reading the experimental results of the AOD water model in the appended reference by Masterson[40].

T. Oake et al.[41] have done extensive experimental studies on the coalescence and break-up of bubbles in swarms with aqueous systems. Their results are in excellent agreement with Sano and Mori[37,38]. They have also studied the region in close proximity of the injection point and found that bubble coalescence is greatest there. In the vicinity right after the bubble detaches from the nozzle, bubble coalescence is the only phenomenon occurring. Bubble break-up does not begin until a position 7 to 10 cm from the nozzle, which is in remarkable agreement with Sano and Mori. Bubble coalescence and break-up occur at an equal rate in the bath at a height greater than 15 cm from the nozzle. These results extrapolated to an AOD vessel indicate that the wear around and above the tuyere may be due to gas expansion and bubble coalescence.

The work of Nakanishi, Fujii, and Szekeley (42) was the first published in which mixing times were correlated to the energy dissipation in steelmaking vessels. They introduced the Index for Selective Carbon Oxidation (ISCO) which is calculated as follows:

$$ISCO = \frac{2Q_{O_2}}{(2Q_{O_2} + Q_D)} \frac{Q_{O_2} t}{W} \quad [10]$$

where Q_{O2} is the oxygen flowrate; Q_D, flowrate of diluent gas; W, weight of melt; and t, mixing time. The first term of the ISCO Index, $2Q_{O2}/(2Q_{O2}+Q_D)$, represents the partial pressure of CO in the melt. The second term of the ISCO Index, $Q_{O2}t/W$, is the ratio of the oxygen supply to the supply of carbon at the reaction site in the melt. In the ISCO Index, the partial pressure of CO, multiplied by the ratio of oxygen supply to carbon supply at the reaction site, is taken to judge the degree of selective oxidation of carbon in the melt. The lower the value of the ISCO Index, the greater the potential to oxidize carbon selectively rather than some other metallic component (e.g., Cr) of the melt.

The total %Fe in the slag as a function of the ISCO Index for various top/bottom steelmaking processes is shown in Figure 5. Clearly, as the ISCO Index decreases, the total %Fe in the slag decreases. A more dramatic correlation has been observed in Cr losses during stainless steel refining. Figure 6 compares Cr losses as a function of ISCO Index for a 5-ton Q-BOP for different operating conditions (the diluent gas was not specified) to a 10-ton AOD. The decrease in Cr losses with a decrease in ISCO Index is very noticeable.

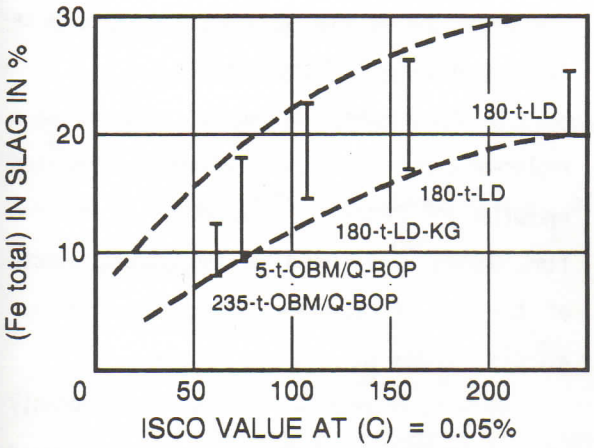

Figure 5. Influence of bath mixing on oxidation of melt. (Nakanishi, Fujii and Szekely (42))

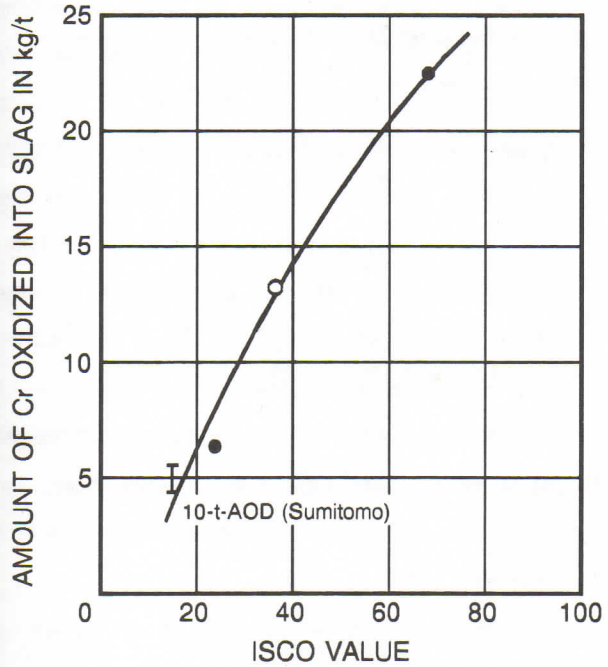

Figure 6. Loss of chromium in slag for 5-ton Q-BOP. (Nakanishi, Fujii and Szekely (42))

Recently, a 5-ton AOD water model was used to measure mixing times as a function of gas flowrate and tuyere placement. For a complete description of this work, see the appended reference by Masterson[40].

Mixing time as a function of flowrate was empirically determined to fit the relation:

$$t = 18.07\ Q^{-.33} \qquad [11]$$

Recalling equation [9], $t \propto Q^{-.33}$, the agreement between experimentally determined functional dependence of the mixing time on the flowrate, Q, is remarkable. Using equation [11], the mixing time in the AOD water model is 17 seconds. There is no data available on the mixing time in AOD vessels, but Kato, et al[43] have measured the mixing time in a 5-ton Q-BOP of 17-20 seconds. The experimental conditions (blow rate, number of tuyeres) were not reported, but it is similar to an AOD vessel, and the agreement is quite good. The agreement between predicted and measured mixing times does support the modeling criteria.

More tangible evidence of good mixing in the AOD is familiar to operators in the form of excellent slag-metal chemical and thermal equilibrium. This excellent mixing aids in the attainment of equilibrium during decarburization, especially at low carbon levels. The increased slag-metal contact promotes predictable, high recovery of alloying elements and rapid, efficient desulfurization.

Stirring is known to improve the kinetics of alloy deoxidation, permitting equilibrium conditions to be more closely approached (44). Extremely low oxide contents are attainable if the oxides formed can escape prior to solidification and if reoxidation is prevented during casting.

C. Degassing

The mechanism of argon degassing is quite similar to that of vacuum degassing. The theoretical aspects of vacuum degassing, particularly with respect to carbon deoxidation, have been aptly discussed in the literature[45,46]. However, there are several inherent differences[47,48] as discussed below.

The removal of dissolved gases from steel by argon results from (1) the effect of argon bubbles in providing nucleation sites for reactions which transfer the dissolved gases from the steel to the gas phase, (2) the improved reaction kinetics resulting from stirring, and (3) the driving force for these reactions provided by the low partial pressure of CO, H_2 and N_2 in the argon bubbles.

During the oxygen blow of AOD refining, evolving carbon monoxide supplements the argon to assist in degassing. The CO and Ar bubbles absorb H_2 and N_2 (as well as CO up to saturation) as they rise through the bath. Argon injection causes considerable stirring of the bath, thus improving the kinetics of the degassing reaction by (1) decreasing the effect of diffusion boundary layers around the reaction sites; (2) transporting the reaction sites to the reactants; and (3) transporting the saturated bubbles away from the newly injected reaction sites.

Degassing in AOD is important not only for the production of low gas content (especially low hydrogen content) low alloy steels but also to control the nitrogen content in stainless steels. Nitrogen will dissolve in steel with deleterious effects in many instances. Consequently, it is often necessary to purge a portion of the dissolved nitrogen by blowing argon through the bath during the latter portion of decarburization and subsequent refining. By switching from nitrogen to argon at some point during the decarburization blow and continuing to use argon during reduction and any subsequent steps, purging of nitrogen by argon and carbon monoxide is accomplished[4]. In order to finish at a specific nitrogen level, the switch-over point from nitrogen to argon must be determined with reasonable accuracy.

In certain grades, on the other hand, nitrogen is desired as a strengthening or austenitizing agent. Production of these steels previously required the addition of expensive nitrogen-bearing ferroalloys; however, these grades can now be made by alloying with gaseous nitrogen at the end of the heat[4].

The first commercial use of nitrogen as a replacement for argon in AOD refining was reported by Moffet and Saccomano[49] in 1972. At the same time, Dokken[50] reviewed the theoretical aspects of the use of nitrogen. Those concepts are discussed in the following paragraphs.

While it is reasonable to use the solubility of nitrogen in pure liquid iron for most plain carbon steels, it is clearly unacceptable in considering stainless grades. The effect of deoxidizing and alloying elements on the activity of carbon, oxygen, nitrogen, and hydrogen has been reported[46,47,51]. For example, the presence of alloying elements such as chromium and vanadium hinder carbon deoxidation and increased nitrogen solubility while the presence of nickel aids the CO reaction and decreases nitrogen solubility. Elements such as titanium and vanadium increase the solubility of nitrogen in steel, thus making its removal more difficult. The formation of stable oxides and/or nitrides inhibit the removal of CO or N_2. For grade 304 stainless steel, the solubility of nitrogen after the AOD reduction step is 0.23%.

The solubility of nitrogen in all steels is known to follow Sievert's Law:

$$\%\underline{N} = \text{const.} \times \sqrt{P_{N_2}} \qquad [12]$$

This relationship is evident from the following reaction and its equilibrium constant:

$$1/2\ N_{2\ (g)} = \underline{N} \qquad [13]$$

$$K_1 = \frac{a_{\underline{N}}}{(P_{N_2})^{0.5}} = \frac{f_{\underline{N}} \cdot \%N}{(P_{N_2})^{0.5}} \qquad [14]$$

where:

$\underline{N}$ represents nitrogen dissolved in the steel

$a_{\underline{N}}$ = The activity of dissolved nitrogen.

$f_{\underline{N}}$ = The activity coefficient of dissolved nitrogen.

$\%\underline{N}$ = The weight percent of dissolved nitrogen.

K_1 = The equilibrium constant of reaction 1.

P_{N_2} = The partial pressure of nitrogen, in atmospheres.

For the AOD, we are interested in P_{N_2} of the exit gas:

$$P_{N2} = \frac{Q_{N_2}}{Q_{N_2} + Q_{Ar} + Q_{CO}} \cdot P_{system}$$

Q_{N_2}, Q_{Ar} = Volumetric flow rate of gas injected

Q_{CO} = Volumetric flow rate of CO generated

Equation [13] clearly reduces to Sievert's Law since $f_{\underline{N}}$ is a constant for a specific bath chemistry and temperature. For the specific case of nitrogen dissolving in pure liquid iron (the binary Fe-N system), the "const." of eqn. [12] is K_1. (Implicit in this statement is: $f_{\underline{N}} = 1$ for Fe-N alloys.)

In pure liquid iron[52], the Gibb's Free Energy for Equation [13] is:

$$\Delta G^\circ_1 = 860 + 5.71\ T\ (cal/g\text{-}atom) \pm 100\ cal \qquad [15]$$

Knowing that $\Delta G^\circ = -RT \ln K$ at equilibrium, we can derive an expression for the logarithm of K_1 in pure liquid iron:

$$\log K_1 = -188/T - 1.25 \qquad [16]$$

At 1600°C (1873°K), the solubility of nitrogen in pure liquid iron is 0.045%. In stainless steels, the activity coefficient of nitrogen is not unity, thus in order to use equation 13, we must calculate $f_{\underline{N}}$.

The effect of alloying elements on the solubility of nitrogen in liquid iron alloys is shown in Figure 7. Notice that the common intercept is the solubility of nitrogen in pure iron discussed above.

A negative interaction coefficient indicates that the alloy element "j" increases the solubility (or decreases the activity) of nitrogen. Conversely, a positive interaction coefficient indicates that the alloy element "j" decreases the solubility (or increases the activity) of $\underline{N}$.

Each curve for a specific element, j, on the diagram defines an activity coefficient of nitrogen in the ternary alloy Fe-N-j. From this activity coefficient, one can determine the interaction coefficient, $e^j_{\underline{N}}$, which describes the effect of the alloy element, j, on the behavior of $\underline{N}$ in the steel. For fundamental work, the reader should consult Wada and Pehlke[54] and their references.

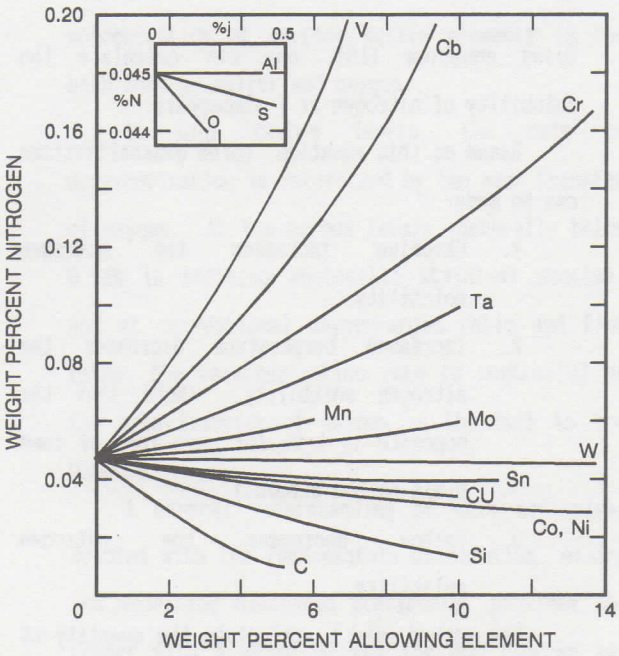

Figure 7. Solubility of nitrogen in alloy melts.

These effects can be combined for a complex alloy such as stainless steel by the equation:[55,56,57]

$$\log f_{\underline{N}} = \left[\frac{3280}{T} - 0.75\right] \sum_{j=1}^{n} e_{\underline{N}}^{j} (\%j) + \sum_{j=1}^{n} r_{\underline{N}}^{j} (\%j)^2 \quad [17]$$

where:

j = an alloy element

$e_{\underline{N}}^{j}$ = interaction coefficient for element j on $\underline{N}$.

$r_{\underline{N}}^{j}$ = second order interaction coefficient for element j on $\underline{N}$.

Table II lists values of interaction coefficients[57]. Notice that $r_{\underline{N}}^{Cr}$ is the only non-zero second order interaction coefficient.

The combined effects of the various alloy elements in most stainless steels may be summarized by the equation:

$$\log \%\underline{N}_{eq} = -188/T - 1.25 - [(3280/T - 0.75)$$

$$(0.13 \times \%C + 0.047 \times \%Si + 0.0 \times \%Ni$$

$$-0.011 \times \%Mo - 0.023 \times \%Mn - 0.047 \times \%Cr)]$$

$$-((+0.00017) \times \%Cr^2) \quad [18]$$

Using equation [18], one can calculate the solubility of nitrogen at 1 atmosphere.

Based on this equation, three generalizations can be made:

1. Chromium increases the nitrogen solubility.
2. Increased temperature decreases the nitrogen solubility. (Note that the opposite is true for pure iron or some plain carbon steels.)
3. Carbon decreases the nitrogen solubility.

The method used to calculate the quantity of argon required to remove dissolved gases has been previously described[47, 58]. The theoretical relationship for the removal of hydrogen and nitrogen with argon degassing in carbon steel is shown in Figure 8. As shown, the amount of argon required to remove hydrogen or nitrogen increases rapidly at low concentration. For example, to reduce hydrogen from 5 ppm to 2.5 ppm requires about 46 ft^3 of argon per ton of carbon steel;

TABLE II
INTERACTION COEFFICIENTS
NITROGEN IN LIQUID IRON AT ABOUT 1600°C

Element, j	$e_{\underline{N}}^{j}$	$r_{\underline{N}}^{j}$
Al	-0.028	
As	+0.018	
B	+0.094	
C	+0.130	
Cb (Nb)	-0.06	
Co	+0.011	
Cr	-0.047	+0.00017
Cu	+0.009	
Mn	-0.023	
Mo	-0.011	
Nb	-0.06	
Ni	+0.010	
O	+0.05	
P	+0.045	
S	+0.007	
Sb	+0.0088	
Se	+0.006	
Si	+0.047	
Sn	+0.007	
Ta	-0.032	
Te	+0.07	
Ti	-0.53	
V	-0.093	
W	-0.0015	
Zn	-0.63	

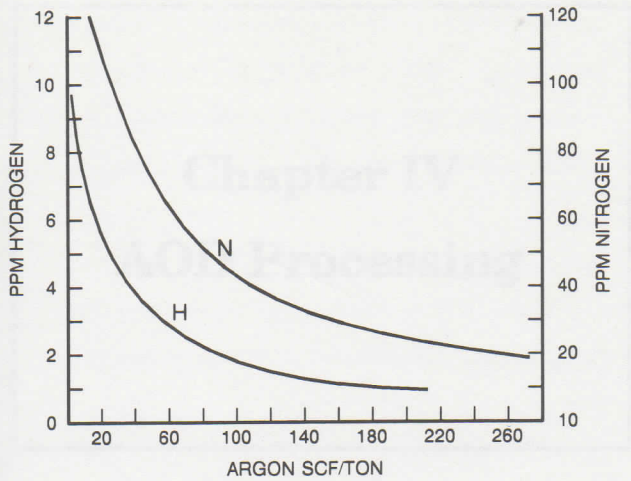

Figure 8. Argon requirement for hydrogen and nitrogen removal at 2912°F. (Houston and Death (58))

however, to go from 3 ppm to 1.5 ppm would require about 72 ft^3 of argon per ton of steel. During decarburization, the significant quantities of CO evolved act as an inert gas with respect to hydrogen and nitrogen and reduce the amount of argon required to remove any given amount of these gases. It is also possible to calculate the amount of inert gases needed to purge nitrogen from stainless steel. For example, to purge dissolved nitrogen from a level of 0.12% to 0.06%, more than 100 ncf of argon/ton of stainless steel is required (assuming 100% efficiency).

Several investigators[59,60,61,62,63] of the kinetics of nitrogen absorption and desorption have indicated that the presence of surface active elements, oxygen and sulfur, serves as a barrier to nitrogen transfer. It is generally accepted that oxygen (or sulfur) will occupy a majority of the surface sites on the gas metal interface preventing the rapid transfer of nitrogen (or other elements) across the interface. Consequently, it is necessary to assume a purging efficiency based on knowledge of the actual conditions in the bath. The proper use of these concepts results in accurate control of nitrogen content in AOD refined steels.

D. Mechanism

While it is beyond the scope of this book to review the mechanism and modeling of decarburization in the AOD process in detail, it is appropriate to make some general comments. The basic reaction model of the AOD process is that oxygen injected through the tuyeres reacts primarily with dissolved carbon, silicon, chromium and manganese in the tuyere zone. The carbon monoxide and the argon (or nitrogen) which was injected with the oxygen as the diluent gas forms a bubble which carries the other oxides through the bath as it ascends. The metallic oxides formed are reduced by carbon and silicon dissolved in the bath as these oxides rise with the bubbles through the melt. Any oxide not reduced while the bubble is in the bath is transferred to the slag phase once the ascending bubble reaches the top of the bath.

Simultaneously, while the gas bubbles ascend, nitrogen, if it is the diluent gas, is absorbed into the melt. Conversely, if argon is the diluent gas, dissolved nitrogen in the melt is desorbed into the bubble. The rates of the nitrogen reaction depends on the mass transfer of nitrogen in the melt and are influenced by the concentration of surface active elements in the bath such as sulfur and oxygen.

At high carbon levels, the rate of decarburization is determined by the mass transfer of oxygen. At low carbon levels (generally below 0.12% in refining austenitic stainless steels), and at conventional oxygen/argon ratio and flow rates, the decarburization rate is controlled by the mass transfer of carbon in the bath to the bubbles.

A general understanding of this mechanism, coupled with the fundamentals of dilution, mixing and degassing discussed previously, provides the reader with a sense of why the AOD process has proven so successful for stainless steel refining.